Article:
Liu, T, Chen, S, Li, K orcid.org/0000-0001-6657-0522 et al. (2 more authors) (2023) Adaptive Multioutput Gradient RBF Tracker for Nonlinear and Nonstationary Regression. IEEE Transactions on Cybernetics. ISSN 2168-2267

https://doi.org/10.1109/TCYB.2023.3235155

Adaptive Multi-Output Gradient RBF Tracker For Nonlinear and Nonstationary Regression

Tong Liu, *Member, IEEE*, Sheng Chen, *Fellow, IEEE*, Kang Li, *Senior Member, IEEE*, Shaojun Gan, Chris J. Harris

***Abstract*—Multi-output regression of nonlinear and nonstationary data is largely under-studied in both machine learning and control communities. This paper develops an adaptive multi-output gradient radial basis function (MGRBF) tracker for online modeling of multi-output nonlinear and nonstationary processes. Specifically, a compact MGRBF network is first constructed with a new two-step training procedure to produce excellent predictive capacity. To improve its tracking ability in fast time-varying scenarios, an adaptive MGRBF (AMGRBF) tracker is proposed, which updates the MGRBF network structure online by replacing the worst performing node with a new node that automatically encodes the newly emerging system state and acts as a perfect local multi-output predictor for the current system state. Extensive experiment results confirm that the proposed AMGRBF tracker significantly outperforms existing state-of-the-art online multi-output regression methods as well as deep-learning based models, in terms of adaptive modeling accuracy and online computational complexity.**

***Index Terms*—Multivariate nonlinear and nonstationary regression, multi-output gradient radial basis function network, two-step training, online adaptive tracking**

I. Introduction

Many real-world systems are nonstationary, and they operate in real-time to continuously produce tremendous amount of data in the form of fast arriving data streams [1]–[3]. A regression model must be capable of adapting to the newly emerging system state within a strictly limited processing time. Recently, there is an increasing trend of applying deep learning to nonlinear regression problem. Typically, deep networks with multilevel feature extraction layers are adopted, such as stacked autoencoder (SAE) [4], [5] or long short-term memory (LSTM) recurrent neural network (RNN) [6], [7]. However, online adaptation of these deep nonlinear models is very challenging if not impossible, since it is prohibitive to adapt large deep networks within a small sampling period in order to track fast time-varying system dynamics.

With the increasing demand for today's complex decision making, the traditional single-output modeling is not coping well with multi-task predictions. Unlike single-output modeling, multi-output modeling takes into account the complex interactions and compound dependencies among the multiple outputs [8], [9]. Multi-output modeling becomes even more challenging under nonstationary environment. Multi-output data gathered from heterogeneous sources come in high speed, and evolve over time with unforeseen drifts. This motivates our current work to develop an effective multi-output online predictive model to deal with fast time-varying characteristics in multivariate data. Existing methods in the literature for online regression can be classified into two groups: multiple local model learning and single nonlinear model learning.

The multiple local model learning strategy has been successfully applied to industrial adaptive soft sensor design in the presence of frequent operating condition deviations [10]–[12]. The essence of this local learning strategy is to partition a nonlinear and nonstationary process into multiple local regions with a moving window. Each region is considered to be stationary and is modeled by a local linear model. The selective ensemble based multiple local model (SEMLM) learning grows local linear models online to automatically identify newly emerged process states, and combines the most up-to-date local models to make an accurate selective ensemble regression (SER) based prediction [13]. The growing and pruning SER (GAP-SER) can further prune the past accumulated local models that are no longer relevant, thus significantly reduce the online computation burden in making prediction [14]. Although the GAP-SER can achieve excellent online prediction performance for modeling nonstationary data, while imposing much less averaged computation time per sample (ACTpS) than the SEMLM, it is still restricted to single-output modeling. The more recent multi-output GAP-SER (MGAP-SER) adopts a novel adaptive local learning strategy based on multivariate statistic that enables growing and pruning multi-output local linear models [15]. Unlike the single-output GAP-SER, the MGAP-SER exploits the complex interactions between multiple output variables, and it attains better prediction accuracy than using multiple single-output GAP-SERs when modeling multi-output processes. A potential drawback common to all multiple local model learning methods is that the size of the SER prediction model constructed changes from sample to sample. It is hard to implement an adaptive controller based on such a variable-size predictor.

The single nonlinear model learning strategy attempts to capture the global nonlinear characteristics from the data using a nonlinear model, such as a neural network. Among various nonlinear models, the radial basis function (RBF) network has become very popular, due to its elegant mathematical formulation, ease of model optimization and strong modeling performance [16]. By formulating the RBF model training as a subset selection problem, the orthogonal least squares (OLS) is used to identify appropriate RBF centers from training

T. Liu is with the Department of Computer Science, The University of Sheffield, Sheffield S1 4DP, U.K. (E-mail: tliu.soton@gmail.com).

S. Chen and C. J. Harris are with School of Electronics and Computer Science, University of Southampton, Southampton SO17 1BJ, UK (E-mails: sqc@ecs.soton.ac.uk, chrisharris57@msn.com). S. Chen is also with Faculty of Information Science and Engineering, Ocean University of China, Qingdao, China

K. Li is with School of Electronic and Electrical Engineering, University of Leeds, Leeds, LS2 9JT, UK (E-mail: K.Li1@leeds.ac.uk)

S. Gan is with Beijing Key Laboratory of Traffic Engineering, College of Metropolitan Transportation, Beijing University of Technology, Beijing 100124, China (E-mail: s.gan@bjut.edu.cn).

This work was supported by the National Natural Science Foundation of China under grant 62003011.

input data, and to estimate output weights simultaneously in an efficient manner [17]–[21]. This procedure can be easily extended to multi-output modeling, where the subset selection is directly based on the trace of the error covariance matrix [22]–[25]. Some other hybrid training algorithms have also been proposed for multi-output RBF (MRBF) model construction [26], [27]. The RBF model typically tracks the changing process dynamics by updating its weight vector using the recursive least square (RLS) algorithm [28]–[30]. However, in a highly time-varying environment, the process dynamics can vary dramatically and weight updating alone is insufficient. Hence, online model structure adaptation is necessary. A typical way of online adapting the RBF structure is to adaptively grow or prune RBF nodes based on their significance, such as resource allocating network (RAN) [31] and growing-and-pruning RBF (GAP-RBF) [32]. Such an approach however produces variable-size nonlinear model, which is not helpful for implementing adaptive controller. To keep a fixed compact-size RBF model, the fast tunable RBF (TRBF) of [33] adjust the individually tunable nodes to track the time-varying process dynamics. Experimental results of [33] show that this TRBF outperforms the RAN and GAP-RBF for online modeling of nonstationary systems.

A novel extension to the RBF network, known as the gradient RBF (GRBF) network, was proposed to deal with time series exhibiting homogeneous nonstationary characteristics [34]. Instead of sensing the trajectory of the series itself, the hidden nodes of the GRBF network react to the gradient of time series. Not surprisingly, this GRBF network trained by the OLS algorithm outperforms the classic RBF network in nonstationary time series prediction [34]. To enhance its adaptive prediction capability for highly nonstationary time series, a fast adaptive GRBF (AGRBF) was proposed for online time series prediction [35], which was further extended to online modeling and identification of nonlinear and time-varying processes in [36]. Similar to the TRBF, during online operation when the current modeling error becomes unacceptable, the AGRBF adapts the model structure by replacing an insignificant node with a new node that automatically encodes the current data. Owing to the local prediction property of the GRBF node, the new node optimization is much more efficient than the TRBF, which imposes little online computation. Extensive experiments of [36] demonstrate that this AGRBF is superior to various existing state-of-the-art adaptive nonlinear models, including the TRBF and GAP-SER, in terms of both online modeling accuracy and computational efficiency. Also the fixed compact-size of AGRBF makes it more applicable in an adaptive control scheme than the GAP-SER.

Although the AGRBF achieves great success in online regression of nonstationary data, it is suitable only for single-output modeling. Due to the particular geometry structure of the GRBF network, we cannot extend it to multi-output modeling by simply adding multiple output neurons to the single-output-neuron GRBF structure, because this does not realize its full predictive capability. Note that this is unlike the MRBF network, which can be obtained by adding the multiple output neurons to the single-output-neuron RBF structure. Also the online adaptive strategies of the AGRBF [36], TRBF [33], RAN [31] and GAP-RBF [32] are all restricted to single-output modeling and they are not applicable to online multi-output modeling. Although we may apply the multiple single-output AGRBF models to identify multi-output systems, this will not only increase the modeling effort considerably but also degrades the achievable online modeling accuracy. Therefore, it is necessary to develop new online adaptive multi-output model by extending the highly desirable GRBF network to multi-output regression. This paper proposes an adaptive multi-output GRBF (AMGRBF) network for tracking nonlinear and nonstationary processes. Our novel contributions are summarized as follows.

1) We propose a new multi-output GRBF (MGRBF) network with excellent predictive capacity for multi-output modeling. Due to the multi-output nature of this new MGRBF structure, the OLS learning cannot be directly applied to model construction. Hence, we further propose a new two-step training method to construct a compact MGRBF model.
2) To improve its tracking ability in highly nonstationary environments, we derive an adaptive mechanism to efficiently adjust the MGRBF model online. During online operation, the MGRBF network adapts its structure by replacing an insignificant node with a new node that automatically encodes the newly emerging system state. This proposed online tracker fully exploits the geometric structure of the MGRBF network, and it is capable of timely capturing the fast-changing process dynamics while maintaining a very low online complexity.
3) Extensive applications of real-world multivariate nonlinear and nonstationary regression demonstrate that the proposed AMGRBF significantly outperforms the existing state-of-the-art online adaptive multi-output models, including the MGAP-SER and the new multi-output TRBF, as well as deep-learning based models.

II. The Proposed MGRBF Network

We consider the generic multi-input multi-output nonlinear time-varying dynamic system that can be represented by the following multivariate nonlinear autoregressive moving average (NARMA) model [25]:

$$\boldsymbol{y}_{t+(K-1)} = \boldsymbol{f}_{\text{sys}}\big(\boldsymbol{x}_t; t\big), \tag{1}$$

where $K \geq 1$ is the prediction step, $\boldsymbol{y}_t = \big[y_{t,1} \cdots y_{t,n_o}\big]^{\mathrm{T}} \in \mathbb{R}^{n_o}$ is the n_o-dimensional system output vector, $\boldsymbol{f}_{\text{sys}}(\bullet; t)$ is the n_o-dimensional unknown and time-varying system mapping, and the overall system input $\boldsymbol{x}_t \in \mathbb{R}^{(n_o n_y + n_i n_u)}$ is given by

$$\boldsymbol{x}_t = \big[\boldsymbol{y}_{t-1}^{\mathrm{T}} \cdots \boldsymbol{y}_{t-n_y}^{\mathrm{T}} \ \boldsymbol{u}_{t-1}^{\mathrm{T}} \cdots \boldsymbol{u}_{t-n_u}^{\mathrm{T}}\big]^{\mathrm{T}}, \tag{2}$$

in which $\boldsymbol{u}_t = \big[u_{t,1} \cdots u_{t,n_i}\big]^{\mathrm{T}} \in \mathbb{R}^{n_i}$ is the n_i-dimensional system input vector, n_y and n_u are the system output and input lags, respectively. Without loss of generality, we focus on one-step-ahead prediction modeling, i.e., $K = 1$. All the results are however equally applicable to the case of $K > 1$.

Two special cases of this NARMA model is the multivariate nonlinear autoregressive (NAR) model or time series

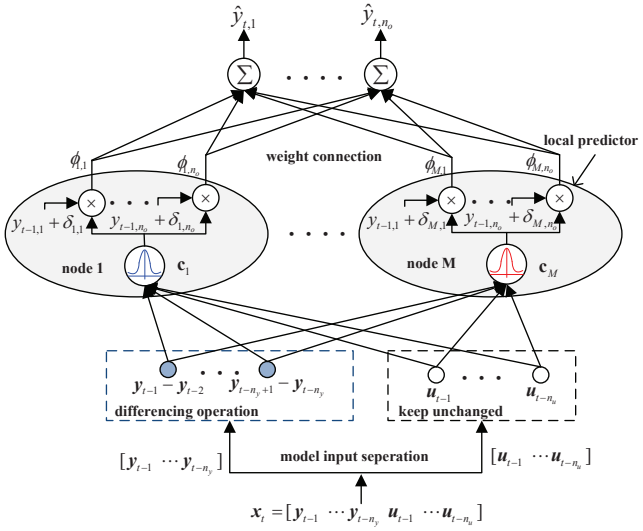

Fig. 1. The proposed MGRBF network structure.

prediction in which $\boldsymbol{x}_t = \left[\boldsymbol{y}_{t-1}^{\mathrm{T}} \cdots \boldsymbol{y}_{t-n_y}^{\mathrm{T}}\right]^{\mathrm{T}}$, and the multivariate nonlinear moving average (NMA) model in which $\boldsymbol{x}_t = \left[\boldsymbol{u}_{t-1}^{\mathrm{T}} \cdots \boldsymbol{u}_{t-n_u}^{\mathrm{T}}\right]^{\mathrm{T}}$.

A. MGRBF Network Structure

The modeling task is to build a prediction model $\widehat{\boldsymbol{y}}_t = \boldsymbol{f}_{\mathrm{mod}}(\boldsymbol{x}_t; \boldsymbol{\Theta})$ to predict $\boldsymbol{y}_t$ given the input $\boldsymbol{x}_t$ of (2), where $\boldsymbol{\Theta}$ denotes the model parameter matrix. We propose a novel MGRBF network, as illustrated in Fig. 1, to perform this task. This MGRBF network is very different from the MRBF network of [22]–[24]. It also has a significant difference with the single-output GRBF network [36].

First, unlike the MRBF network, the input layer of the MGRBF network automatically differences the past outputs in $\boldsymbol{x}_t$ to yield the actual network input vector $\boldsymbol{x}'_t \in \mathbb{R}^{n_c}$ as

$$\boldsymbol{x}'_t = \left[(\boldsymbol{y}_{t-1} - \boldsymbol{y}_{t-2})^{\mathrm{T}} \cdots (\boldsymbol{y}_{t-n_y+1} - \boldsymbol{y}_{t-n_y})^{\mathrm{T}} \ \boldsymbol{u}_{t-1}^{\mathrm{T}} \cdots \boldsymbol{u}_{t-n_u}^{\mathrm{T}}\right]^{\mathrm{T}}, \tag{3}$$

where $n_c = (n_o(n_y - 1) + n_i n_u)$. Differencing helps to eliminate trend and seasonality, and makes the series less time-dependent [37]. For the NAR regression task, the input vector $\boldsymbol{x}_t$ does not contain the past system outputs, and the MGRBF network will not implement this difference operation.

Also a MGRBF hidden node is very different from that of the single-output GRBF network. Specifically, unlike the single-output GRBF network, where each Gaussian node's response is modified by a single-output local predictor, the n_o local predictors are required in each MGRBF hidden node. Let M be the number of the hidden nodes in the MGRBF network. Observe from Fig. 1 that each MGRBF hidden node contains the n_o local one-step predictors that modify the Gaussian node's response. The response of ith local predictor in the jth MGRBF node to the input vector $\boldsymbol{x}'_t$ is given by

$$\phi_{j,i}(\boldsymbol{x}'_t) = \exp\left(\frac{-\|\boldsymbol{x}'_t - \boldsymbol{c}_j\|^2}{2\sigma^2}\right) \times \left(y_{t-1,i} + \delta_{j,i}\right), \quad \text{for } i = 1, \cdots, n_o, \ j = 1, \cdots, M, \tag{4}$$

where σ is the width of Gaussian kernel, which is typically set as the maximum Euclidean distance among nodes [38], $\boldsymbol{c}_j \in \mathbb{R}^{n_c}$ is the node center, and $\delta_{j,i}$ is a scalar associated with the ith local predictor of the jth node. It can be observed from (4) that the multiple local predictors in the hidden node share the same Gaussian center $\boldsymbol{c}_j$, but with different multiplication terms $\left(y_{t-1,i} + \delta_{j,i}\right)$, $1 \le i \le n_o$. The term $\left(y_{t-1,i} + \delta_{j,i}\right)$ can be interpreted as a local one-step prediction of $y_{t,i}$ by the ith local predictor. The essence of MGRBF node is that if the input vector $\boldsymbol{x}'_t$ is very similar to the jth center $\boldsymbol{c}_j$, the value of the jth Gaussian function is close to 1 and all the local predictors $\left(y_{t-1,i} + \delta_{j,i}\right)$ for $1 \le i \le n_o$ become fully active.

The output layer of the MGRBF network consists of the n_o output nodes, which form the n_o linear combiners of the M hidden layer responses to produce the model output vector $\widehat{\boldsymbol{y}}_t = \left[\widehat{y}_{t,1} \cdots \widehat{y}_{t,n_o}\right]^{\mathrm{T}} \in \mathbb{R}^{n_o}$. Let $\boldsymbol{\phi}_{t,j} \in \mathbb{R}^{n_o}$ be the response vector of the jth node to $\boldsymbol{x}'_t$, i.e.,

$$\boldsymbol{\phi}_{t,j} = \left[\phi_{j,1}(\boldsymbol{x}'_t) \cdots \phi_{j,n_o}(\boldsymbol{x}'_t)\right]^{\mathrm{T}}, \tag{5}$$

and denote the connection weight vector from the jth hidden node's response vector to the ith output node as

$$\boldsymbol{\theta}_{i,j} = \left[\theta_{i,j,1} \cdots \theta_{i,j,n_o}\right]^{\mathrm{T}}. \tag{6}$$

Then the ith output of the MGRBF network is given by

$$\widehat{y}_{t,i} = \sum_{j=1}^{M} \boldsymbol{\phi}_{t,j}^{\mathrm{T}} \boldsymbol{\theta}_{i,j}. \tag{7}$$

Further define the overall response vector $\boldsymbol{\varphi}_{\bar{M},t} \in \mathbb{R}^{\bar{M}}$ of the hidden layer to the input $\boldsymbol{x}'_t$ as

$$\boldsymbol{\varphi}_{\bar{M},t}^{\mathrm{T}} = \left[\boldsymbol{\phi}_{t,1}^{\mathrm{T}} \cdots \boldsymbol{\phi}_{t,M}^{\mathrm{T}}\right], \tag{8}$$

where $\bar{M} = n_o M$, as well as the overall output layer connection matrix $\boldsymbol{\Theta}_{\bar{M} \times n_o} \in \mathbb{R}^{\bar{M} \times n_o}$

$$\boldsymbol{\Theta}_{\bar{M} \times n_o} = \begin{bmatrix} \boldsymbol{\theta}_{1,1} & \boldsymbol{\theta}_{2,1} & \cdots & \boldsymbol{\theta}_{n_o,1} \\ \boldsymbol{\theta}_{1,2} & \boldsymbol{\theta}_{2,2} & \cdots & \boldsymbol{\theta}_{n_o,2} \\ \vdots & \vdots & \ddots & \vdots \\ \boldsymbol{\theta}_{1,M} & \boldsymbol{\theta}_{2,M} & \cdots & \boldsymbol{\theta}_{n_o,M} \end{bmatrix}. \tag{9}$$

The output vector of the MGRBF network to $\boldsymbol{x}'_t$ is given by

$$\widehat{\boldsymbol{y}}_t^{\mathrm{T}} = \boldsymbol{\varphi}_{\bar{M},t}^{\mathrm{T}} \boldsymbol{\Theta}_{\bar{M} \times n_o}. \tag{10}$$

Remark 1: Hidden neuron node in all the existing neural network architectures produces single response to the input. By contrast, hidden neuron node in our MGRBF network produces multiple response to the input. This represents an innovative idea in the artificial neural network design.

B. Two-Step Training of MGRBF

The task of building a MGRBF model is to choose appropriate centers $\boldsymbol{c}_j$, and scalars $\boldsymbol{\delta}_j = \left[\delta_{j,1} \cdots \delta_{j,n_o}\right]^{\mathrm{T}}$ based on the given set of training inputs and outputs $\{\boldsymbol{x}'_t; \boldsymbol{d}_t, \boldsymbol{y}_t\}_{t=1}^{N}$, where N is the total number of training samples, and

$$\boldsymbol{d}_t = \boldsymbol{y}_t - \boldsymbol{y}_{t-1}. \tag{11}$$

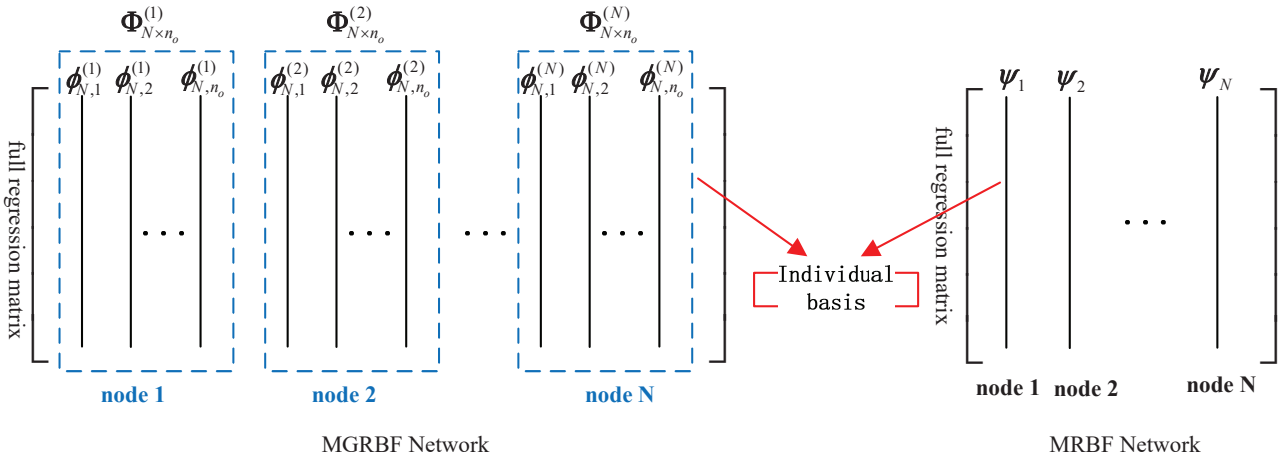

Fig. 2. Difference of the regression matrices between the MGRBF network and the RBF/MRBF/GRBF network.

Specifically, we choose the centers $\boldsymbol{c}_j$, $1 \le j \le M$, from the training input data $\{\boldsymbol{x}'_t\}_{t=1}^N$. In particular, if $\boldsymbol{x}'_t$ is selected as the jth center $\boldsymbol{c}_j$, we set $\boldsymbol{\delta}_j = \boldsymbol{d}_t$ to ensure that the jth hidden node response $\boldsymbol{\phi}_{t,j}$ is a perfect local predictor of $\boldsymbol{y}_t$. Thus by considering every data point $(\boldsymbol{x}'_t, \boldsymbol{d}_t)$ as a candidate hidden node, the problem of constructing the MGRBF network is equivalent to the task of selecting a M-term subset model $\{\boldsymbol{c}_j, \boldsymbol{\delta}_j\}_{j=1}^M$ from the full N-term model $\{\boldsymbol{x}'_t, \boldsymbol{d}_t\}_{t=1}^N$.

Formally, by using every $(\boldsymbol{x}'_t, \boldsymbol{d}_t)$ as a candidate hidden node, we obtain the full N-hidden-node MGRBF network with the overall output layer connection matrix $\boldsymbol{\Theta}_{\bar{N}\times n_o} \in \mathbb{R}^{\bar{N}\times n_o}$, where $\bar{N} = n_o N$, as well as the overall response matrix $\boldsymbol{\Phi}_{N\times\bar{N}} \in \mathbb{R}^{N\times\bar{N}}$ of the hidden layer to the inputs $\{\boldsymbol{x}'_t\}_{t=1}^N$

$$\boldsymbol{\Phi}_{N\times\bar{N}} = \begin{bmatrix} \boldsymbol{\varphi}_{\bar{N},1}^{\mathrm{T}} \\ \boldsymbol{\varphi}_{\bar{N},2}^{\mathrm{T}} \\ \vdots \\ \boldsymbol{\varphi}_{\bar{N},N}^{\mathrm{T}} \end{bmatrix} = \left[\boldsymbol{\Phi}_{N\times n_o}^{(1)} \ \boldsymbol{\Phi}_{N\times n_o}^{(2)} \cdots \boldsymbol{\Phi}_{N\times n_o}^{(N)}\right], \quad (12)$$

where $\boldsymbol{\Phi}_{N\times n_o}^{(l)} \in \mathbb{R}^{N\times n_o}$ is the response matrix of the lth candidate node whose center vector is $\boldsymbol{c}_l = \boldsymbol{x}'_l$ and scalar vector is $\boldsymbol{\delta}_l = \boldsymbol{d}_l$. Since each hidden node contains n_o local predictors and N hidden nodes are employed to form the full MGRBF model, the size of regression matrix is $N \times \bar{N}$. For $1 \le l \le N$, $\boldsymbol{\Phi}_{N\times n_o}^{(l)}$ can be expressed as

$$\boldsymbol{\Phi}_{N\times n_o}^{(l)} = \left[\boldsymbol{\phi}_{N,1}^{(l)} \ \boldsymbol{\phi}_{N,2}^{(l)} \cdots \boldsymbol{\phi}_{N,n_o}^{(l)}\right] \quad (13)$$

with $\boldsymbol{\phi}_{N,i}^{(l)} = \left[\phi_{l,i}(\boldsymbol{x}'_1) \cdots \phi_{l,i}(\boldsymbol{x}'_N)\right]^{\mathrm{T}}$ being the response of the ith local predictor of the lth node to $\{\boldsymbol{x}'_t\}_{t=1}^N$. Constructing the M-term MGRBF network $\{\boldsymbol{c}_j, \boldsymbol{\delta}_j\}_{j=1}^M$ for $M \ll N$ becomes a subset selection problem of selecting the M matrix bases $\left\{\boldsymbol{\Phi}_{N\times n_o}^{(l_j)}\right\}_{j=1}^M$ from the full regression matrix $\boldsymbol{\Phi}_{N\times\bar{N}}$.

Remark 2: Note that this subset selection problem is very different from constructing a M-term MRBF network. The latter task is to select a subset of the M basis vectors from the full set of the N basis vectors, and the multi-output OLS algorithm [22]–[24] can readily be applied to efficiently solve this subset selection problem. By contrast, our current subset selection problem is to select a subset of M basis matrices from the full set of the N basis matrices, and it is mathematically infeasible to directly employ the OLS to select these basis matrices from the candidate pool. Fig. 2 highlights this main difference of the two subset selection tasks by displaying the full regression matrices or candidate pools for these two tasks. Also the hybrid constructive algorithms of [26], [27] cannot be used to train the MGRBF network. To the authors' best knowledge, we are not aware any existing subset selection algorithm which can select subset matrix bases.

We propose to solve the problem of constructing the MGRBF network by separating it into two parts. First, we select appropriate centers from the training data set $\{\boldsymbol{x}'_t; \boldsymbol{y}_t\}_{t=1}^N$. This subset selection problem can be formulated as the problem of constructing an 'equivalent' M-term MRBF network with the OLS algorithm. Second, with the selected centers $\{\boldsymbol{c}_j = \boldsymbol{x}'_{t_j}\}_{j=1}^M$ from the constructed MRBF model, their associated scalar vectors are assigned to $\{\boldsymbol{\delta}_j = \boldsymbol{d}_{t_j}\}_{j=1}^M$ so as to complete the MGRBF hidden layer. The output weight matrix of this constructed M-node MGRBF network is finally solved by the regularized least square (LS) estimation method. This two-step construction procedure is detailed as follows.

OLS based center selection: The aim is to select the M center vectors of the the MGRBF network from the training data set. This is equivalent to construct a M-node subset MRBF network with the OLS algorithm. By using every input data $\boldsymbol{x}'_t$ as a candidate center vector, we can model the training data set $\{\boldsymbol{x}'_t; \boldsymbol{y}_t\}_{t=t}^N$ with the full N-node MRBF network as

$$\boldsymbol{Y}_{N\times n_o} = \boldsymbol{\Psi}_{N\times N}\boldsymbol{\Theta}_{N\times n_o} + \boldsymbol{E}_{N\times n_o}, \quad (14)$$

where $\boldsymbol{\Theta}_{N\times n_o} \in \mathbb{R}^{N\times n_o}$ is the output-layer connection weight matrix of the full N-node MRBF network, and $\boldsymbol{\Psi}_{N\times N} \in \mathbb{R}^{N\times N}$ is the corresponding full regression matrix given by

$$\boldsymbol{\Psi}_{N\times N} = \left[\boldsymbol{\psi}_1 \ \boldsymbol{\psi}_2 \cdots \boldsymbol{\psi}_N\right] = \begin{bmatrix} \psi_{1,1} & \psi_{1,2} & \cdots & \psi_{1,N} \\ \psi_{2,1} & \psi_{2,2} & \cdots & \psi_{2,N} \\ \vdots & \vdots & \ddots & \vdots \\ \psi_{N,1} & \psi_{N,2} & \cdots & \psi_{N,N} \end{bmatrix} \quad (15)$$

in which $\psi_{t,j}$ denotes the response of the jth node to $\boldsymbol{x}'_t$, while

$$\boldsymbol{Y}_{N\times n_o} = \begin{bmatrix} \boldsymbol{y}_1^{\mathrm{T}} \\ \vdots \\ \boldsymbol{y}_N^{\mathrm{T}} \end{bmatrix} \in \mathbb{R}^{N\times n_o}, \quad (16)$$

and $\boldsymbol{E}_{N\times n_o}\in\mathbb{R}^{N\times n_o}$ is the modeling residual matrix.

Let the orthogonal decomposition of $\boldsymbol{\Psi}_{N\times N}$ be

$$\begin{aligned}\boldsymbol{\Psi}_{N\times N} =&\boldsymbol{W}_{N\times N}\boldsymbol{A}_{N\times N}\\ =&\begin{bmatrix}\boldsymbol{w}_1 & \boldsymbol{w}_2\cdots\boldsymbol{w}_N\end{bmatrix}\begin{bmatrix}1 & a_{1,2} & \cdots & a_{1,N}\\ 0 & 1 & \cdots & a_{2,N}\\ \vdots & \ddots & \ddots & \vdots\\ 0 & \cdots & 0 & 1\end{bmatrix}\end{aligned} \tag{17}$$

with orthogonal columns that satisfy $\boldsymbol{w}_i^{\mathrm{T}}\boldsymbol{w}_j=0$, for $i\neq j$. The space spanned by the set of bases $\{\boldsymbol{w}_j\}$ is the same space spanned by the bases $\{\boldsymbol{\psi}_j\}$, and (14) can be rewritten as

$$\boldsymbol{Y}_{N\times n_o} =\boldsymbol{W}_{N\times N}\boldsymbol{G}_{N\times n_o}+\boldsymbol{E}_{N\times n_o}, \tag{18}$$

where the weight matrix $\boldsymbol{G}_{N\times n_o}$ for the space spanned by the columns of $\boldsymbol{W}_{N\times N}$, namely,

$$\boldsymbol{G}_{N\times n_o}=\begin{bmatrix}g_{1,1} & \cdots & g_{1,n_o}\\ \vdots & \ldots & \vdots\\ g_{N,1} & \cdots & g_{N,n_o}\end{bmatrix} \tag{19}$$

is linked to the weight matrix $\boldsymbol{\Theta}_{N\times n_o}$ by the triangular system $\boldsymbol{A}_{N\times N}\boldsymbol{\Theta}_{N\times n_o}=\boldsymbol{G}_{N\times n_o}$. The classic Gram-Schmidt method can be used to perform this orthogonal decomposition [22].

For multi-output case, the contribution of a candidate basis to the trace of the desired output covariance matrix is used to define how significant this basis is, and the trace of the covariance of $\boldsymbol{Y}_{N\times n_o}$ can be expressed as [22]–[24]

$$\begin{aligned}\mathrm{tr}\left(\boldsymbol{Y}_{N\times n_o}^{\mathrm{T}}\boldsymbol{Y}_{N\times n_o}/N\right) =&\sum_{j=1}^{N}\Big(\sum_{i=1}^{n_o}g_{j,i}^2\Big)\boldsymbol{w}_j^{\mathrm{T}}\boldsymbol{w}_j/N\\ &+\mathrm{tr}\big(\boldsymbol{E}_{N\times n_o}^{\mathrm{T}}\boldsymbol{E}_{N\times n_o}/N\big).\end{aligned} \tag{20}$$

The error reduction ratio due to $\boldsymbol{w}_k$ can be defined as

$$[\mathrm{err}]_k=\frac{\big(\sum_{i=1}^{n_o}g_{k,i}^2\big)\boldsymbol{w}_k^{\mathrm{T}}\boldsymbol{w}_k}{\mathrm{tr}(\boldsymbol{Y}_{N\times n_o}^{\mathrm{T}}\boldsymbol{Y}_{N\times n_o})}, 1\le k\le N. \tag{21}$$

Based on this radio, significant nodes can be selected in a forward regression procedure. At the kth step of the selection procedure, a candidate node with the largest value of $[\mathrm{err}]_k$ is selected, from among the rest of $N-k+1$ candidates. The selection procedure is terminated when $1-\sum_{j=1}^{M}[\mathrm{err}]_j$ is smaller than a pre-set threshold, and this yields a regression model with M hidden nodes or centers $\{\boldsymbol{c}_j=\boldsymbol{x}'_{t_j}\}_{j=1}^{M}$.

MGRBF construction and weight estimation: After the significant centers $\{\boldsymbol{c}_j=\boldsymbol{x}'_{t_j}\}_{j=1}^{M}$ have been obtained, they are used as the centers of the M-node MGRBF network, and the associated scalar vectors are assigned as $\{\boldsymbol{\delta}_j=\boldsymbol{d}_{t_j}\}_{j=1}^{M}$. This completes the construction of the hidden layer of the MGRBF network. To determine the output layer connection matrix $\boldsymbol{\Theta}_{\bar{M}\times n_o}$ of the constructed MGRBF network, express the network output matrix to the inputs $\{\boldsymbol{x}'_t\}_{t=1}^{N}$ by

$$\widehat{\boldsymbol{Y}}_{N\times n_o} =\boldsymbol{\Phi}_{N\times\bar{M}}\boldsymbol{\Theta}_{\bar{M}\times n_o}, \tag{22}$$

where $\boldsymbol{\Phi}_{N\times\bar{M}}$ is the hidden-layer response matrix. We can calculate the weight matrix $\boldsymbol{\Theta}_{\bar{M}\times n_o}$ by minimizing the regularized LS cost function

$$J=\left\|\boldsymbol{Y}_{N\times n_o}-\widehat{\boldsymbol{Y}}_{N\times n_o}\right\|^2+\lambda\left\|\boldsymbol{\Theta}_{\bar{M}\times n_o}\right\|^2, \tag{23}$$

where $\lambda\ge 0$ is the regularization parameter. Typically, a small positive λ is used, and $\lambda=0$ corresponds to no regularization. The closed-formed regularized LS solution of (23) is given by

$$\boldsymbol{\Theta}_{\bar{M}\times n_o}=\big(\boldsymbol{\Phi}_{N\times\bar{M}}^{\mathrm{T}}\boldsymbol{\Phi}_{N\times\bar{M}}+\lambda\boldsymbol{I}_{\bar{M}}\big)^{-1}\boldsymbol{\Phi}_{N\times\bar{M}}^{\mathrm{T}}\boldsymbol{Y}_{N\times n_o}, \tag{24}$$

where $\boldsymbol{I}_{\bar{M}}$ denotes the $\bar{M}\times\bar{M}$ identity matrix.

III. MGRBF Tracker

With the above two-step training procedure, we can construct a compact MGRBF network by including the most significant training data states to accurately modeling the training data. Each selected hidden-node center encodes a significant system state from the training data and the node response vector is a perfect local predictor for the system output related to this system state. In a time-varying scenario, however, the process dynamics can vary dramatically and new data states may emerge, making some of the past data dynamics encoded in the hidden nodes of the MGRBF network obsolete. Therefore, it is vital for the MGRBF network to forget the most out-of-date old system states encoded in the hidden layer so as to free up space for capturing the newly emerged data dynamics as fast as these new states appear.

The single-output AGRBF [36] adopts an effective online adaptive strategy to address the above-mentioned problem. Specifically, it carries out weight updating at every sampling time as usual. If the prediction performance of the GRBF network becomes unacceptable, it replaces the hidden node that contributes the least with a new node to capture the newly emerging data dynamics. We modify this effective adaptive strategy to be suitable for the MGRBF network, and propose the MGRBF *tracker*, which contains the *weight adaptation* and *tunable node adaptation* components.

A. Weight Adaptation

The weight matrix $\boldsymbol{\Theta}_{\bar{M}\times n_o}$ of the MGRBF network can be simply updated by the RLS algorithm to track smooth data variations. At sample t, given $\boldsymbol{x}'_t$, the MGRBF network produces the output according to (10) as

$$\widehat{\boldsymbol{y}}_t =\boldsymbol{\Theta}_{\bar{M}\times n_o,t-1}^{\mathrm{T}}\boldsymbol{\varphi}_{\bar{M},t} \tag{25}$$

where $\boldsymbol{\Theta}_{\bar{M}\times n_o,t-1}$ is the weight matrix obtained at sample $t-1$. Then the prediction error $\boldsymbol{e}_t\in\mathbb{R}^{n_o}$ is given as

$$\boldsymbol{e}_t =\boldsymbol{y}_t-\boldsymbol{\Theta}_{\bar{M}\times n_o,t-1}^{\mathrm{T}}\boldsymbol{\varphi}_{\bar{M},t}. \tag{26}$$

The RLS algorithm adapts the weight matrix according to

$$\begin{cases}\boldsymbol{g}_t=\boldsymbol{\Gamma}_{t-1}\boldsymbol{\varphi}_{\bar{M},t}\big(\gamma+\boldsymbol{\varphi}_{\bar{M},t}^{\mathrm{T}}\boldsymbol{\Gamma}_{t-1}\boldsymbol{\varphi}_{\bar{M},t}\big)^{-1},\\ \boldsymbol{\Gamma}_t=\big(\boldsymbol{\Gamma}_{t-1}-\boldsymbol{g}_t\boldsymbol{\varphi}_{\bar{M},t}^{\mathrm{T}}\boldsymbol{\Gamma}_{t-1}\big)\gamma^{-1},\\ \boldsymbol{\Theta}_{\bar{M}\times n_o,t}=\boldsymbol{\Theta}_{\bar{M}\times n_o,t-1}+\boldsymbol{g}_t\boldsymbol{e}_t^{\mathrm{T}},\end{cases} \tag{27}$$

where $\boldsymbol{g}_t\in\mathbb{R}^{\bar{M}}$ is the Kalman gain vector, $0.9\le\gamma<1$ is the forgetting factor, and $\boldsymbol{\Gamma}_t\in\mathbb{R}^{\bar{M}\times\bar{M}}$ is the inverse of the covariance matrix which is usually initialized to $\boldsymbol{\Gamma}_0=\vartheta\boldsymbol{I}_{\bar{M}}$ with ϑ being a large positive constant.

B. Tunable Node Adaptation

The RLS weight adaptation itself is insufficient under a highly nonstationary environment. When the MGRBF network performs poorly, the current MGRBF structure will need updating. The normalized average output error is used to measure the MGRBF performance at every sampling time

$$\widetilde{e}_t = \|\boldsymbol{e}_t\|^2 / \|\boldsymbol{y}_t\|^2. \tag{28}$$

Based on this metric, we have the following criterion

$$\begin{cases} \text{if } \widetilde{e}_t < \varepsilon: \ \text{MGRBF structure unchanged,} \\ \text{if } \widetilde{e}_t \geq \varepsilon: \ \text{worst node replaced by new node,} \end{cases} \tag{29}$$

where ε is a pre-set threshold. In general, the smaller ε is, the better modeling accuracy can be achieved, but the more frequent node replacement may occur.

When $\widetilde{e}_t \geq \varepsilon$, the worst node with the least contribution to the overall performance is replaced with a new one. The contribution of a node is revealed by its sum of squared weighted local predictor outputs, which is defined by

$$\mathit{contri}_j = \sum_{i=1}^{n_o} \left(\boldsymbol{\phi}_{t,j}^{\mathrm{T}} \boldsymbol{\theta}_{i,j}\right)^2, \ 1 \leq j \leq M. \tag{30}$$

We find the node with the smallest *contri*

$$m = \arg \min_{1 \leq j \leq M} \mathit{contri}_j, \tag{31}$$

and replaced it by a new node. Since each MGRBF hidden node contains a center and n_o local predictor scalars, they need to be replaced together.

The center $\boldsymbol{c}_m$ and scalars $\boldsymbol{\delta}_m$ of the new replacement node can be determined or 'optimized' easily by exploiting the geometric property of MGRBF hidden node, similar to the AGRBF [35], [36]. Specifically, we simply set $\boldsymbol{c}_m = \boldsymbol{x}'_t$ and $\boldsymbol{\delta}_m = \boldsymbol{d}_t$ to ensure that the new replacement node m encodes the newest data state and is a perfect local multi-output predictor of $\boldsymbol{y}_t$. Since the set of centers now contain a new one, the Gaussian width σ needs to be updated based on the new maximum Euclidean distance among the centers.

After the new node is determined, the weight matrix of the updated network needs to be recalculated. We use the p latest data $\{\boldsymbol{x}_{t-i}, \boldsymbol{y}_{t-i}\}_{i=0}^{p-1}$ to compute the regularized LS estimate

$$\boldsymbol{\Theta}_{\bar{M} \times n_o, t} = \left(\boldsymbol{\Phi}_{p \times \bar{M}, t}^{\mathrm{T}} \boldsymbol{\Phi}_{p \times \bar{M}, t} + \lambda \boldsymbol{I}_{\bar{M}}\right)^{-1} \boldsymbol{\Phi}_{p \times \bar{M}, t}^{\mathrm{T}} \boldsymbol{Y}_{p \times n_o, t}, \tag{32}$$

where the desired output matrix $\boldsymbol{Y}_{p \times n_o, t} \in \mathbb{R}^{p \times n_o}$ and the regression matrix $\boldsymbol{\Phi}_{p \times \bar{M}, t} \in \mathbb{R}^{p \times \bar{M}}$ are given respectively by

$$\boldsymbol{Y}_{p \times n_o, t} = \begin{bmatrix} \boldsymbol{y}_t^{\mathrm{T}} \\ \boldsymbol{y}_{t-1}^{\mathrm{T}} \\ \vdots \\ \boldsymbol{y}_{t-p+1}^{\mathrm{T}} \end{bmatrix}, \ \boldsymbol{\Phi}_{p \times \bar{M}, t} = \begin{bmatrix} \boldsymbol{\varphi}_{\bar{M}, t}^{\mathrm{T}} \\ \boldsymbol{\varphi}_{\bar{M}, t-1}^{\mathrm{T}} \\ \vdots \\ \boldsymbol{\varphi}_{\bar{M}, t-p+1}^{\mathrm{T}} \end{bmatrix}. \tag{33}$$

In general, the number of the latest data p trades off estimation accuracy and tracking performance. For severely drifting or nonstationary data streams, a small p is preferred.

If the tunable node adaptation takes place at sample t, the RLS weight updating (27) does not take place. Instead the weight matrix is updated with the regularized LS estimate (32), and we need to initialize the inverse covariance matrix to

$$\boldsymbol{\Gamma}_t = \left(\boldsymbol{\Phi}_{p \times \bar{M}, t}^{\mathrm{T}} \boldsymbol{\Phi}_{p \times \bar{M}, t} + \lambda \boldsymbol{I}_{\bar{M}}\right)^{-1}. \tag{34}$$

This ensures a smooth transition from one adaptation mode to another at the next sample.

Algorithm 1 Adaptive MGRBF Tracker

1: **Two-step training**: Construct M-node MGRBF network from N-sample training set with centers and local predictors $\{\boldsymbol{c}_j, \boldsymbol{\delta}_j\}_{j=1}^{M}$ and weight matrix $\boldsymbol{\Theta}_{\bar{M} \times n_o}$.
2: **Hyperparameters**: Node replacement threshold ε, bandwidth p, regularization parameter λ, forgetting factor γ.
3: **Initialization**: Set sample index $t = 1$, $\boldsymbol{\Gamma}_{t-1} = \vartheta \boldsymbol{I}_{\bar{M}}$, $\boldsymbol{\Theta}_{\bar{M} \times n_o, t-1} = \boldsymbol{\Theta}_{\bar{M} \times n_o}$.
4: **Online prediction**: Given $\boldsymbol{x}'_t$, compute MGRBF network prediction $\widehat{\boldsymbol{y}}_t$ with (25).
5: **Online adaptation**: When $\boldsymbol{y}_t$ is available, compute $\widetilde{e}_t$ with (26) and (28).
6: **IF** $\widetilde{e}_t < \varepsilon$: *Weight adaptation* mode
7: Update weight matrix to $\boldsymbol{\Theta}_{\bar{M} \times n_o, t}$ with RLS (27).
8: **ELSE IF** $\widetilde{e}_t \geq \varepsilon$: *Tunable node adaptation* mode
9: Compute contributions for all M nodes with (30).
10: Find worst node m with (31), and replace it with new node by setting $\boldsymbol{c}_m = \boldsymbol{x}'_t$ and $\boldsymbol{\delta}_m = \boldsymbol{y}_t - \boldsymbol{y}_{t-1}$.
11: Compute new Gaussian width σ with new maximum Euclidean distance among centers.
12: Use p latest data $\{\boldsymbol{x}_{t-i}, \boldsymbol{y}_{t-i}\}_{i=0}^{p-1}$ to compute weight matrix $\boldsymbol{\Theta}_{\bar{M} \times n_o, t}$ with regularized LS estimate (32).
13: Calculate $\boldsymbol{\Gamma}_t$ according to (34).
14: **END IF**
15: Set $t = t + 1$ and go to step 4.

C. Algorithm Summary

The proposed MGRBF tracker is summarized in Algorithm 1. During the online operation, our MGRBF tracker adapts the model according to the current environment. If the process undergoes smooth variation, it operates only by the weight adaptation with the RLS algorithm. When abrupt changes occur in the system, it updates the model structure by replacing the worst performing node with the new one that automatically encodes the newly emerged data state and acts as the perfect local predictor of the current system output.

From a learning perspective, our MGRBF tracker achieves a balanced trade-off between the 'stability' and 'plasticity' [35]. Specifically, it retains the acquired knowledge in the hidden layer of the MGRBF network (stability), with each node encoding an independent local data state learned from the history. At the same time, it adapts to new knowledge with a fast recovery (plasticity) – every time when a new system state emerges, it 'frees' the memory by 'forgetting' the most out-of-date knowledge to encode the newly emerged knowledge. It can be seen that our MGRBF tracker is designed to have fast tracking capability for accurately capturing the underlying characteristics of nonstationary data, while maintaining low online computation complexity.

IV. Numerical Experiments

We perform extensive experiments, including modeling of real-world river flow time series as well as two industrial soft sensor applications, to evaluate the proposed MGRBF network. Two metrics, the mean square error (MSE) and the determinant of the error covariance $\log(\det(\mathrm{Cov}(\boldsymbol{E})))$ over the test data, are utilized to evaluate each single-output and multi-outputs online modeling performance, respectively. Additionally, the coefficient of determination (R^2) is also utilized. Since each output has a R^2 value, the averaged R^2 over all the outputs is used to evaluate the multi-outputs modeling performance. The online computation complexity of an adaptive model is quantified by ACTpS. The computer for carrying out the experiments has the following configuration: Windows 10, 16 GB of RAM, CPU i7-9750 (2.60 GHz), and Matlab version R2018b.

A. State-of-the-Art Benchmarks

We compare with the following state-of-the-art benchmarks.

1) MGAP-SER [15], consisting of multi-output local model growing and pruning as well SER based online multi-output predictor, is a powerful multiple local model learning approach for multi-output nonstationary data modeling. The window size W, bandwidth p and threshold ξ are the three algorithmic parameters, and their influence on the modeling performance can be found in [13]–[15].
2) Multi-output TRBF (MTRBF) is an extension of the single-output TRBF [33] to adaptive multi-output modeling. During online operation, it adopts a similar adaptive mechanism of [33] to replace the worst performing node with a new node. This new node replacement is achieved by iterative gradient descent optimization to determine the new center. Hence, the MTRBF imposes much higher online complexity than our MGRBF tracker. We empirically set the step size and the number of iterations for gradient descend to 0.1 and 5, respectively. The node replacement threshold ε and bandwidth p are the two algorithmic parameters to be determined.
3) Multiple AGRBFs: We also employ the multiple (n_o) AGRBFs, one for each output of the multi-output systems in our experiments. The node replacement threshold ε and bandwidth p are the two algorithmic parameters, and their sensitivity analysis can be found in [35], [36].
4) SAE is a deep network that learns hierarchical feature representations from data with multilevel feature layers [4], [5], [39], [40]. First, multiple autoencoders (AEs) are pre-trained in an unsupervised way layer by layer. After pre-training, a linear regression layer with multi-output neurons is added on the top of the stacked AEs, and the whole SAE is trained by the stochastic gradient descend algorithm. The trained SAE is fixed during online operation, since it is impractical to adapt it in real-time.
5) LSTM is a variant of RNN that is designed to extract dynamic temporal information from data [6], [7], [41]–[43]. For the LSTM with single hidden layer and multi-output neurons, Adam optimizer [44] is used to train the model based on the MSE cost. The trained LSTM is fixed during online operation, as it is impossible to adapt it in real-time.
6) MRBF is a non-adaptive version of MTRBF. A compact MRBF network is constructed by the multi-output OLS algorithm [22]–[24] during the training, and the trained model is fixed during online prediction.
7) Multiple LSSVMs: a least-squares support-vector machine (LSSVM) is a least-squares version of the SVM [45]–[48]. The trained multiple LSSVMs are fixed during online prediction, as it is difficult to adapt them online.
8) Multiple RVMs: The relevance vector machine (RVM) has a similar form to the SVM but requires fewer kernel functions and provides higher sparseness [49]–[52], which is computationally more efficient than the SVM for modeling. The trained RVMs are fixed during online prediction, as it is difficult to adapt them in real-time.

For the LSSVM and RVM, the Gaussian function is adopted as their nonlinear kernels. For the adaptive models, the forgetting factor of the RLS algorithm is set to $\gamma = 0.98$, and the regularization parameter is set to $\lambda = 0.001$. Other important hyperparameters are chosen carefully and empirically, as detailed in the following case studies.

B. River Network Flow Time Series

The river flow domain is a temporal prediction task designed to test predictions on the flows in a river network for 48 hours in the future at specific locations [53]. The datasets were obtained from US National Weather Service and include hourly flow observations for eight sites in Mississippi River network in the United States from September 2011 to September 2012. This domain is a natural candidate for multi-target regression because there are clear physical relationships between readings in the contiguous river network [53]. We select the 4 sites in the river network with time-lagged observations from 6, 18 and 36 hours in the past as the model inputs

$$\begin{aligned}\boldsymbol{x}_t = &\big[y_{t-6,1}\ y_{t-18,1}\ y_{t-36,1}\ y_{t-6,2}\ y_{t-18,2}\ y_{t-36,2}\\ &\cdots y_{t-6,4}\ y_{t-18,4}\ y_{t-36,4}\big]^{\mathrm{T}} \in \mathbb{R}^{12},\end{aligned} \tag{35}$$

to predict the river flows at the 4 sites 48 hours in the future

$$\boldsymbol{y}_{t+48} = \big[y_{t+48,1}\ y_{t+48,2}\ y_{t+48,3}\ y_{t+48,4}\big]^{\mathrm{T}} \in \mathbb{R}^4. \tag{36}$$

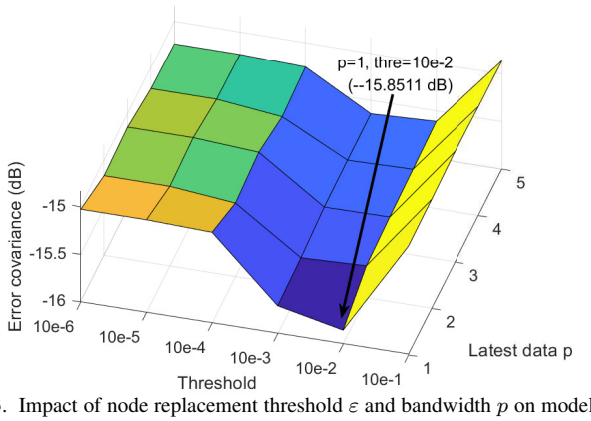

Fig. 3. Impact of node replacement threshold ε and bandwidth p on modeling performance of adaptive MGRBF for river flow prediction.

TABLE I
TEST PERFORMANCE COMPARISON OF MRBF, MULTIPLE LSSVMS, MULTIPLE RVMS, LSTM, SAE, MGAP-SER, MTRBF, MULTIPLE AGRBFS AND PROPOSED METHOD FOR RIVER FLOW PREDICTION.

Methods	Nodes/models	MSE (dB)				$\log(\det(\mathrm{Cov}(\boldsymbol{E})))$	averaged R^2	ACTpS (ms)
		site 1	site 2	site 3	site 4			
MRBF	10	-16.0189	-11.2589	-12.8737	-18.7931	-8.0962	-1.4443	NA
multiple (4) LSSVMs	NA	-6.9514	-15.6354	-15.8206	-18.9504	-7.7754	-2.0772	NA
multiple (4) RVMs	NA	-10.7052	-10.5302	-10.5785	-12.9145	-7.3356	-4.5478	NA
LSTM	32	-11.8314±1.4558	-10.4837±1.4551	-13.8334±0.5648	-17.2837±2.2197	-7.6419±0.1807	-2.2374±0.7302	NA
SAE	[9, 6, 3]	-6.3909±2.1459	-7.9033±4.0252	-15.1941±2.0442	-9.7459±5.6262	-6.8673±0.5025	-14.1398±3.6912	NA
MGAP-SER	56 to 57	-41.0089	-34.3093	-40.1263	-36.9421	-15.2414	0.9841	2.6661
MTRBF	10	-40.6812	-34.9584	-40.4439	-36.4690	-15.6787	0.9836	0.8272
multiple AGRBFs	10×4	**-41.5132**	**-36.5974**	**-41.4592**	**-37.1300**	**-15.6840**	**0.9866**	**0.5284**
Proposed	10	**-41.7907**	**-36.2358**	**-42.6381**	**-37.1156**	**-15.8511**	**0.9867**	**0.1159**

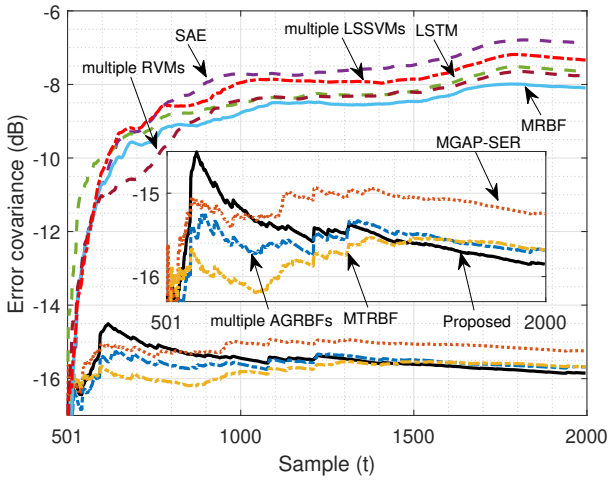

Fig. 4. Comparison of test $\log(\det(\mathrm{Cov}(\boldsymbol{E})))$ learning curves of various models for river flow prediction.

From the 4 sites, 2000 samples are collected with the first 500 samples as the training set and the remaining 1500 samples for online prediction and adaptive modeling.

The sizes of the MTRBF and each AGRBF network are empirically chosen to be $M=10$, as suggested in [35], [36]. Hence, the $n_o=3$ AGRBFs have a total of 40 hidden nodes. For a fair comparison, the MRBF and our proposed method also have a network size of $M=10$. The node replacement threshold ε and bandwidth p are two key algorithmic parameters for the proposed method, and we conduct a grid search, yielding the results depicted in Fig. 3. According to Fig. 3, we set $\varepsilon = 10e-2$ and $p=1$ for our method. The node replacement thresholds are empirically chosen to be $10e-2$ and $10e-3$ for the AGRBFs and MTRBF, respectively, while their bandwidths are both set to be 1. We set the window size $W=50$, bandwidth $p=5$ and threshold $\xi=0.4$ for the MGAP-SER empirically. The LSTM network has 32 hidden nodes, and the structure of the SAE model is $[9,6,3]$. The learning rate and training epochs for both the SAE and LSTM are 0.001 and 200, respectively. The Gaussian kernel widths for the LSSVM and RVM are set to 1 and 10, respectively.

The online prediction performance by the 9 models are tabulated in Table I, and their online error covariance learning curves are compared in Fig. 4. It is well-known that the performance of deep neural networks, such as SAE and LSTM, depend on initialization. Therefore, the average MSEs and $\log(\det(\mathrm{Cov}(\boldsymbol{E})))$ over 20 independent experiments together with the corresponding standard deviations are listed in Table I for the SAE and LSTM. Observe that the nonadaptive methods, including the MRBF, multiple LSSVMs, multiple RVMs, LSTM and SAE, are the worst models, as evidenced by their large test $\log(\det(\mathrm{Cov}(\boldsymbol{E})))$. In Table I, black boldface value indicates the best performance and blue boldface value indicates the second best one. Observe from Fig. 4 that all the adaptive models significantly outperform the nonadaptive models, while our method exhibits the fastest reduction in the error covariance among the adaptive models. The test prediction accuracies achieved by the four adaptive models are quite close, but our method is undoubtedly the winner, in terms of both online prediction accuracy and computational complexity. In particular, its ACTpS is only 0.1159 ms, which is nearly five times smaller than the second best multiple AGRBFs. Fig. 5 depicts the river flow prediction results by the proposed method, which clearly demonstrates that our method is capable of effectively capturing the real-time time-varying dynamics of the river flows in the four different sites.

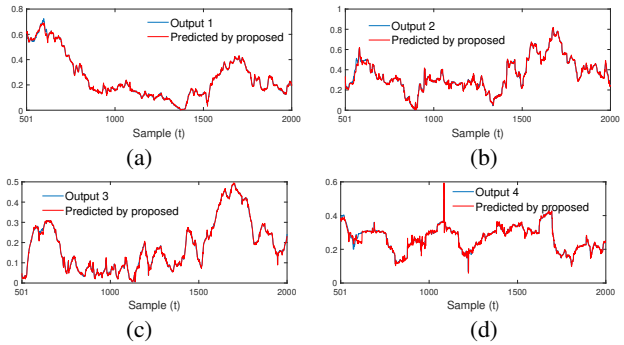

Fig. 5. Online prediction of river network flows by proposed adaptive MGRBF: (a) site 1, (b) site 2, (c) site 3 and (d) site 4.

C. Sulfur Recovery Unit Process

The sulfur recovery unit (SRU) [54] is used to remove environment pollutions from the acid gas streams. Specifically,

TABLE II
VARIABLE DESCRIPTION IN SRU PROCESS.

Input and output variables	Description
$u_{t,1}$	MEA gas flow
$u_{t,2}$	First air flow
$u_{t,3}$	Second air flow
$u_{t,4}$	Gas flow in SWS zone
$u_{t,5}$	Air flow in SWS zone
$y_{t,1}$	Concentration of H_2S
$y_{t,2}$	Concentration of SO_2

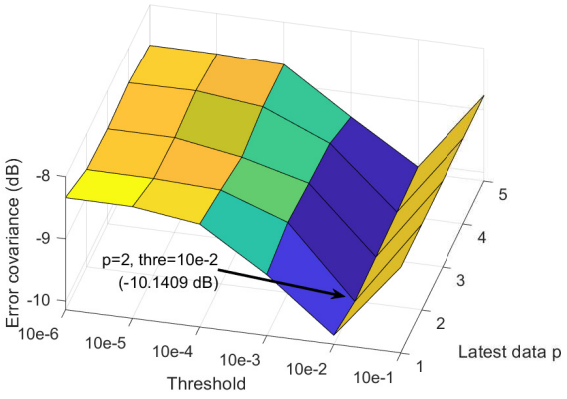

Fig. 6. Impact of node replacement threshold ε and bandwidth p on modeling performance of adaptive MGRBF for online modeling of SRU process.

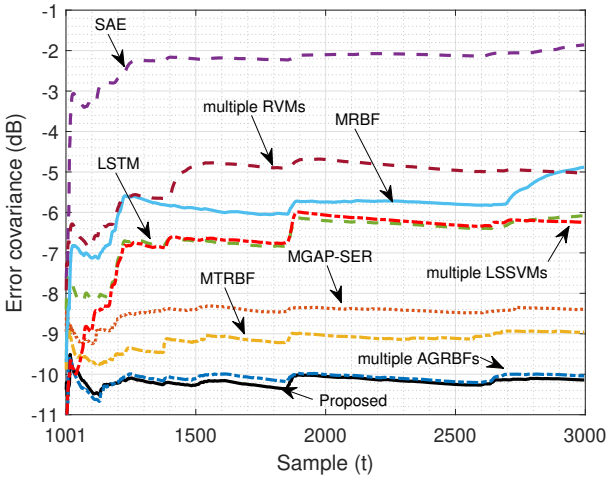

Fig. 7. Comparison of test $\log(\det(\mathrm{Cov}(\boldsymbol{E})))$ learning curves of various models for online modeling of SRU process.

it is widely used in petrochemical industry to recover H_2S as elemental sulfur through the Claus reaction:

$$2H_2S + SO_2 \rightleftharpoons 3S + 2H_2O$$

The sulfur recovery rate of the Claus process is about 95% to 97%. The tail gas normally contains unrecovered sulfur H_2S and SO_2, which are harmful to human health. Therefore, their concentrations must be properly monitored before released to atmosphere. However, these two kinds of acid gas can seriously damage hardware sensors by corrosion and consequently the hardware instruments are frequently removed for maintenance. To avoid this costly maintenance and to provide continuously monitoring, soft sensors are often employed to estimate the concentrations of H_2S and SO_2 online. Five process variables and the concentrations of H_2S and SO_2 are considered as the process inputs and outputs for the soft sensor, which are tabulated in Table II.

Based on expert knowledge and physical insight, the input vector to the SRU process can be expressed as [54]

$$\begin{aligned}\boldsymbol{x}_t =&\big[u_{t,1}\ u_{t-5,1}\ u_{t-7,1}\ u_{t-9,1}\ u_{t,2}\cdots\\ &u_{t-9,4}\ u_{t,5}\ u_{t-5,5}\ u_{t-7,5}\ u_{t-9,5}\big]^{\mathrm{T}} \in \mathbb{R}^{20},\end{aligned} \tag{37}$$

and the process output vector is $\boldsymbol{y}_t = \big[y_{t,1}\ \ y_{t,2}\big]^{\mathrm{T}} \in \mathbb{R}^2$. Because the $\boldsymbol{x}_t$ does not contain the past system output, we have $\boldsymbol{x}'_t = \boldsymbol{x}_t$. Total 3000 samples are collected from the SRU dataset, among which the first 1000 samples are used for training and and the rest of 2000 samples for online prediction.

Similarly, we set node replacement threshold $\varepsilon = 10e-2$ and bandwidth $p = 2$ for the proposed method according to Fig. 6. The node replacement thresholds are set to be $10e-2$ and $10e-3$ for the AGRBFs and MTRBF, respectively, while their bandwidths are both set to be 2. We set window size $W = 90$, bandwidth $p = 4$ and threshold $\xi = 0.9$ for the MGAP-SER by trail and error. The LSTM network has 128 hidden nodes, and the structure of the SAE model is $[15, 10, 7]$. The structure parameters for the MRBF, LSSVM, RVM, LTSM and SAE are identical with the previous simulation.

Table III lists the online prediction results attained by the 9 models, and Fig. 7 compares their online learning curves. The average R^2 of the SAE is extremely poor, as it can hardly predict this process. Our method attains slightly better prediction accuracy than the second best AGRBFs, while imposing a ACTpS half of the later. The MGAP-SER and MTRBF achieve comparable performance, but the former costs much higher computation time. Again, the nonadaptive models are inferior to the adaptive models. The online prediction results of H_2S and SO_2 by our method are shown in Fig. 8, which again demonstrates its excellent tracking capacity.

The aforementioned results are the one-step-head predictive models' performance. Our proposed method is equally applicable to the multi-step prediction, similarly to the other multi-output adaptive models. We further compare the multi-step ahead prediction performance of three multi-output adaptive models, namely, the MGAP-SER, MTRBF and our proposed method in Fig. 9. It is evident that the proposed method con-

TABLE III
TEST PERFORMANCE COMPARISON OF MRBF, MULTIPLE LSSVMS, MULTIPLE RVMS, LSTM, SAE, MGAP-SER, MTRBF, MULTIPLE AGRBFS AND PROPOSED METHOD FOR ONLINE MODELING OF SRU PROCESS.

Methods	Nodes/models	MSE (dB)		$\log(\det(\mathrm{Cov}(\boldsymbol{E})))$ (dB)	averaged R^2	ACTpS (ms)
		H_2S	SO_2			
MRBF	10	-22.6132	-21.9699	-4.8827	-4.5430	NA
multiple (2) LSSVMs	NA	-24.5532	-22.9210	-5.0276	-2.8162	NA
multiple (2) RVMs	NA	-31.5518	-27.1409	-6.2441	0.0009	NA
LSTM	128	-29.9898±0.7944	-26.7115±1.6079	-6.0864±0.1645	-0.3132±0.2427	NA
SAE	[15, 10, 7]	-9.2133±5.1917	-1.1580±3.9066	-1.8591±0.9642	-465.627±459.5	NA
MGAP-SER	97 to 99	-43.6743	-39.9716	-8.3931	0.9434	2.5112
MTRBF	10	-46.5586	-42.4370	-8.9619	0.9695	0.6439
multiple AGRBFs	10×2	**-51.0393**	**-48.7857**	**-10.0409**	**0.9910**	**0.0683**
Proposed	10	**-51.4999**	**-48.7655**	**-10.1409**	**0.9915**	**0.0344**

TABLE IV
TEST PERFORMANCE COMPARISON OF MRBF, MULTIPLE LSSVMS, MULTIPLE RVMS, LSTM, SAE, MGAP-SER, MTRBF, MULTIPLE AGRBFS AND PROPOSED METHOD FOR ONLINE MODELING OF WWTP.

Methods	Nodes/models	MSE (dB)			$\log(\det(\mathrm{Cov}(\boldsymbol{E})))$ (dB)	averaged R^2	ACTpS (ms)
		S_{ND}	X_{ND}	Flow rate			
MRBF	10	-31.9835	-36.7155	-12.0979	-8.8920	0.6646	NA
multiple (3) LSSVMs	NA	-25.9981	-27.8330	-12.0723	-8.6290	0.6392	NA
multiple (3) RVMs	NA	-31.5492	-35.9096	-11.6451	-8.8968	0.6276	NA
LSTM	64	-29.5306±0.7073	-29.8652±1.7440	-10.4257±0.1561	-8.1325±0.1170	0.5000±0.0167	NA
SAE	[5, 4, 3]	-29.1925±6.7376	-36.7223±5.7536	-9.8310±0.7487	-9.9372± 0.8495	0.4233±0.0832	NA
MGAP-SER	209 to 210	**-67.3247**	**-49.5914**	17.4971	-9.9418	-299.0	4.8829
MTRBF	10	-34.2170	-35.8245	**-30.6560**	**-10.0960**	**0.9909**	**0.0907**
multiple AGRBFs	10×3	-31.8713	-35.3647	-26.3281	-9.4047	0.9809	0.3084
Proposed	10	**-34.7267**	**-38.0835**	**-31.5260**	**-10.5854**	**0.9927**	**0.0600**

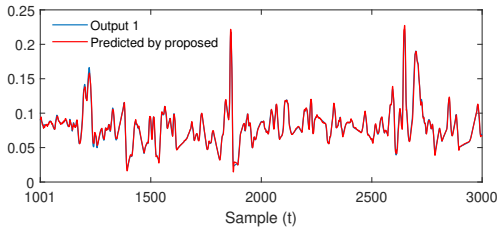

(a)

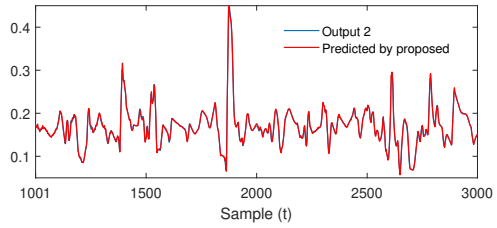

(b)

Fig. 8. Online modeling of SRU process by adaptive MGRBF: (a) H_2S, and (b) SO_2.

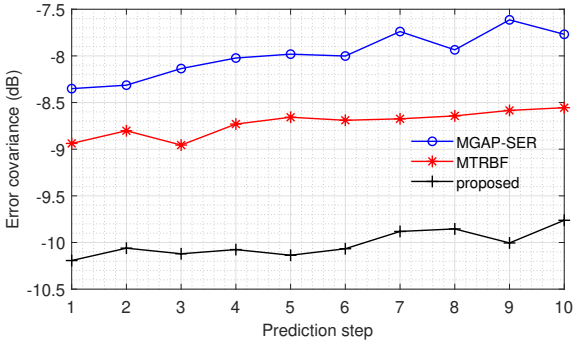

Fig. 9. Comparison of multi-step-ahead prediction performance for SRU process by MGAP-SER, MTRBF and proposed method.

sistently outperforms the other two methods at any prediction step. In terms of online computational complexity, a multi-step-ahead predictor has similar ACTpS as its one-step-ahead counterpart. The best multi-step-ahead prediction accuracy and the lowest online computational complexity together with a fixed compact network size makes our adaptive MGRBF network ideal for adaptive controller implementation.

D. Wastewater Treatment Plant

Wastewater treatment plant (WWTP) [55] is a large nonlinear and time-varying system subject to large perturbations in influent flow rate and pollutant load, together with uncertainties concerning the composition of the incoming wastewater.

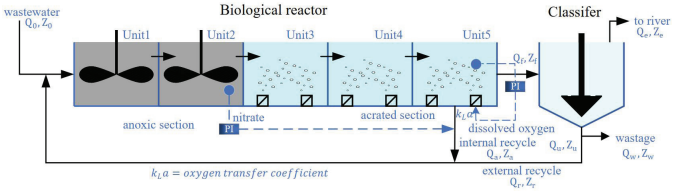

Fig. 10. Schematic overview of WWTP.

As shown in Fig. 10, the benchmark plant contains a five-compartment activated sludge reactor consisting of two anoxic tanks followed by three aerobic tanks. The activated sludge reactor is followed by a secondary clarifier. The aim of this process is to remove organic matter and to perform nitrification and denitrification. The purpose of this study is to establish an adaptive multi-output soft sensor to simultaneously estimate the soluble biodegradable organic nitrogen S_{ND}, particulate biodegradable organic nitrogen X_{ND} and flow rate, which are three key variables. The process inputs and outputs are listed in Table V. Hence, the process input vector is

$$\boldsymbol{x}_t = \left[u_{t,1}\ u_{t,2}\ u_{t,3}\ u_{t,4}\ u_{t,5}\right]^{\mathrm{T}} \in \mathbb{R}^5, \tag{38}$$

and the process output vector is

$$\boldsymbol{y}_t = \left[y_{t,1}\ y_{t,2}\ y_{t,3}\right]^{\mathrm{T}} \in \mathbb{R}^3. \tag{39}$$

The influent data are collected under severe weather condition (a combination of dry weather and a long rain period), which makes the underlying process dynamics strongly nonstationary and imposes an enormous challenge on the performance of soft sensor [56]. We collect 1300 samples from the WWTP dataset, among which the first 500 samples are used for training, while the rest of them are for online prediction.

TABLE V
VARIABLE DESCRIPTION IN THE WWTP.

Input and output variables	Description
$u_{t,1}$	Readily biodegradable substrate
$u_{t,2}$	Particulate inert organic matter
$u_{t,3}$	Slowly biodegradable substrate
$u_{t,4}$	Active heterotrophic biomass
$u_{t,5}$	$NH_4^+ + NH_3$ nitrogen
$y_{t,1}$	S_{ND}
$y_{t,2}$	X_{ND}
$y_{t,3}$	Flow rate

Again, we carefully set all algorithmic parameters of the 9 models by trail and error. From Fig. 11, the node replacement threshold and bandwidth for the proposed method are set

to $\varepsilon = 10e-2$ and $p = 2$, respectively. The MTRBF has the identical algorithmic parameter settings with the proposed method, while the AGRBFs choose $\varepsilon = 10e-1$ and $p = 1$ to achieve the best performance. For the MGAP-SER, we set window size $W = 15$, bandwidth $p = 1$ and threshold $\xi = 0.9$. The LSTM network has 64 hidden nodes, and the structure of the SAE model is $[5, 4, 3]$. The MRBF, LSSVM and RVM have the identical structure settings with the previous simulation.

Table IV presents online modeling performance achieved by the 9 models, and Fig. 12 compares their online error covariance learning curves. The results again show that our proposed method achieves the best online estimation accuracy while imposing the lowest computational complexity. It is interesting to observe that although the MGAP-SER attains the smallest MSEs for estimating $\mathrm{S_{ND}}$ and $\mathrm{X_{ND}}$, its flow rate prediction is the worst among all the models, which is also reflected in its extremely poor average R^2. This may be due to that the local multi-output linear models of the MGAP-SER do not handle the severe nonlinear relationship between the multiple output variables. The SAE achieves a comparable performance with the MGAP-SER and is slightly better than the multiple AGRBFs. However, its performance has a large fluctuation. Another interesting phenomenon can be seen from Fig. 12 is that the performance of all the 9 models degrade significantly at nearly 800 samples. This can be explained from Fig. 13, which depicts the three process outputs. It can be clearly seen that all the three process outputs experience abrupt changes around $t = 800$, particularly for the flow rate. As mentioned before, this dataset is collect under severe weather condition, and this abrupt drift can be contributed to the abrupt weather changes. The online prediction results of $\mathrm{S_{ND}}$, $\mathrm{X_{ND}}$ and flow rate by our method are depicted in Fig. 13, in comparison with the three true outputs of the WWTP. The results of Fig. 13 clearly demonstrates the excellent tracking capacity of the proposed MGRBF tracker.

Since multi-step ahead process control is essential for WWTP, we also compare the multi-step ahead prediction performance of the three adaptive multi-output models, and the results are presented in Fig. 14. Again, our method consistently outperforms the other two methods. Our method has the additional advantage of imposing the lowest online computational burden.

Experimental results involving three real-world multi-output

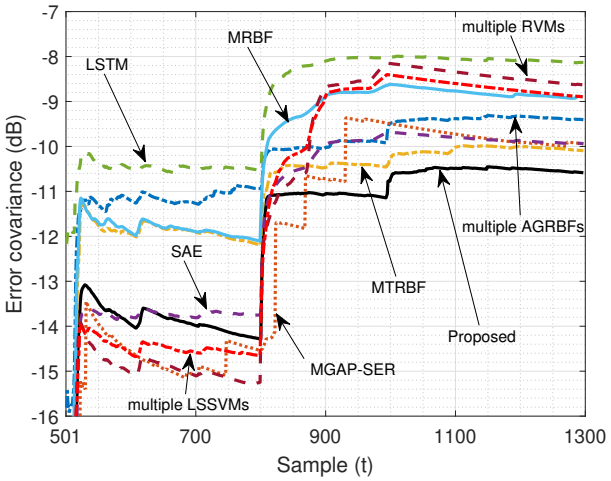

Fig. 12. Comparison of test $\log(\det(\mathrm{Cov}(\boldsymbol{E})))$ learning curves of various models for online modeling of WWTP.

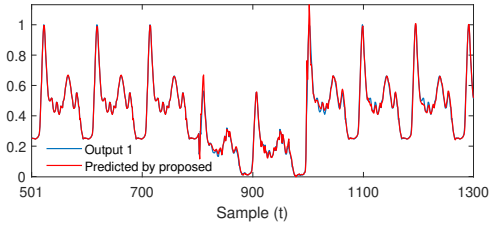

(a)

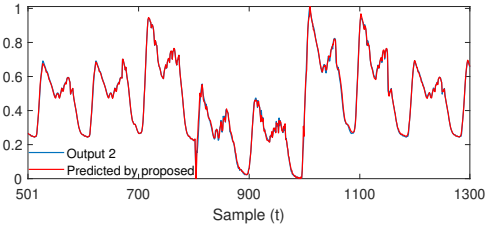

(b)

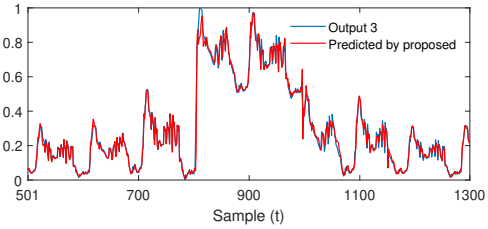

(c)

Fig. 13. Online modeling of WWTP by adaptive MGRBF: (a) $\mathrm{S_{ND}}$, (b) $\mathrm{X_{ND}}$ and (c) Flow rate.

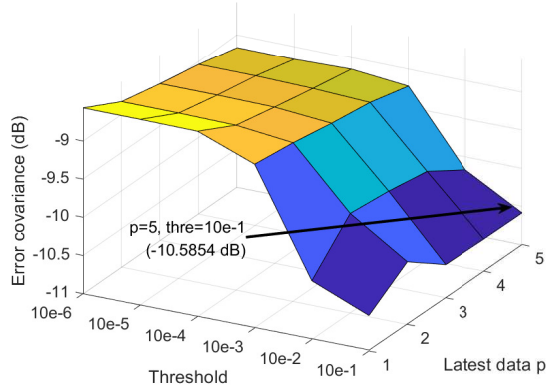

Fig. 11. Impact of node replacement threshold ε and bandwidth p on modeling performance of adaptive MGRBF for online modeling of WWTP.

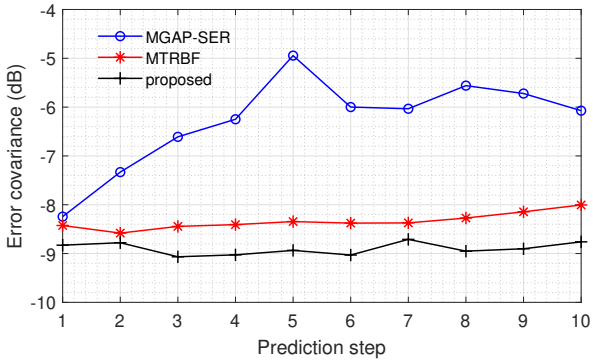

Fig. 14. Comparison of multi-step-ahead prediction performance for WWTP by the MGAP-SER, MTRBF and proposed method.

nonlinear and nonstationary processes demonstrate that the proposed adaptive MGRBF tracker achieves the state-of-the-art adaptive modeling performance. Our method not only consistently attains the best tracking accuracy but also imposes very low computational complexity in online adaptation. Unlike adopting multiple single-output AGRBFs, our method is capable of capturing the complex interactions among the multiple process outputs and simultaneously tracking fast time-varying dynamics of the different process outputs. Moreover, the proposed method has excellent multi-step-ahead prediction capability, which is highly desired for nonlinear model predictive control design.

V. Conclusions

We have proposed a novel adaptive MGRBF network for online modeling of multi-output nonlinear and time-varying processes. First, we have designed a new MGRBF network structure with strong multi-output predictive modeling capacity. A two-step training procedure has been proposed to construct a compact MGRBF network, with each hidden node encoding an independent data state and acting as a perfect local predictor of the system output vector corresponding to this system state. Second, we have designed a new adaptive tracking mechanism to efficiently adapt the MGRBF network in real time. Specifically, during online operation, the MGRBF tracker replaces the worst performing node with a new one that automatically captures the newly emerged process state. Extensive experiments involving real-world river network flow time-series prediction and two industrial soft sensor applications have demonstrated that our proposed adaptive MGRBF model outperforms the existing state-of-the-art online multi-output modeling methods, in terms of both online prediction accuracy and computation complexity. Our results have also confirmed that state-of-the-art online adaptive models are superior over nonadaptive deep neural networks for online adaptive modeling of multivariate nonlinear and fast time-varying data. With the advantages of excellent adaptive modeling capability and very low online computational complexity together with small fixed-size network structure, our proposed adaptive MGRBF network offers an ideal platform for implementing adaptive nonlinear control scheme.

In addition to nonlinear and nonstationary characteristics, many real-world systems are high dimensional with strong correlations among variables. A popular way to deal with high dimensionality is to employ deep-learning models to extract deep latent features from raw data. Due to the complex architecture of deep neural networks, it is difficult to adapt them online to track fast time-varying data dynamics. Hence, the integration of deep-learning models with the proposed adaptive MGRBF offers an important future research direction for handling high-dimensional nonlinear and nonstationary data tracking.

References

[1] G. Ditzler, M. Roveri, C. Alippi, and R. Polikar, "Learning in non-stationary environments: A survey," *IEEE Computational Intelligence Mag.*, vol. 10, no. 4, pp. 12–25, Nov. 2015.

[2] I. Skrjanc, *et al.*, "Evolving fuzzy and neuro-fuzzy approaches in clustering, regression, identification, and classification: A survey," *Information Sciences*, vol. 490, pp. 344–368, Jul. 2019.

[3] J. L. Lobo, *et al.*, "Evolving spiking neural networks for online learning over drifting data streams," *Neural Networks*, vol. 108, pp. 1–19, Dec. 2018.

[4] G. E. Hinton and R. R. Salakhutdinov, "Reducing the dimensionality of data with neural networks," *Science*, vol. 313, no. 5786, pp. 504–507, Jul. 2006.

[5] W. Yan, D. Tang, and Y. Lin "A data-driven soft sensor modeling method based on deep learning and its application," *IEEE Trans. Industrial Electronics*, vol. 64, no. 5, pp. 4237–4245, May 2017.

[6] S. Hochreiter and J. Schmidhuber, "Long short-term memory," *Neural Computation*, vol. 9, no. 8, pp. 1735–1780, Nov. 1997.

[7] X. Yuan, L. Li, and Y. Wang, "Nonlinear dynamic soft sensor modeling with supervised long short-term memory network," *IEEE Trans. Industrial Informatics*, vol. 16, no. 5, pp. 3168–3175, May 2020.

[8] D. Xu, *et al.*, "Survey on multi-output learning," *IEEE Trans. Neural Networks and Learning Systems*, vol. 31, no. 7, pp. 2409–2429, Jul. 2020.

[9] H. Borchani, G. Varando, C. Bielza, and P. Larranaga, "A survey on multi-output regression," *Data Mining Knowledge Discovery*, vol. 5, no. 5, pp. 216–233, 2015.

[10] P. Kadlec and B. Gabrys, "Local learning-based adaptive soft sensor for catalyst activation prediction," *AIChE J.*, vol. 57, no. 5, pp. 1288–1301, May 2011.

[11] W. Shao, *et al.*, "Online soft sensor design using local partial least squares models with adaptive process state partition," *Chemometrics and Intelligent Laboratory Systems*, vol. 144, pp. 108–121, May 2015.

[12] W. Shao, S. Chen, and C. J. Harris, "Adaptive soft sensor development for multi-output industrial processes based on selective ensemble learning," *IEEE Access*, vol. 6, pp. 55628–55642, Oct. 2018.

[13] T. Liu, S. Chen, S. Liang, and C.J. Harris, "Selective ensemble of multiple local model learning for nonlinear and nonstationary systems," *Neurocomputing*, vol. 378, pp. 98–111, Feb. 2020.

[14] T. Liu, S. Chen, S. Liang, and C.J. Harris, "Growing and pruning selective ensemble regression for nonlinear and nonstationary systems," *IEEE Access*, vol. 8, no. 1 pp. 73278–73292, Apr. 2020.

[15] T. Liu, *et al.*, "Multi-output selective ensemble identification of nonlinear and nonstationary industrial processes," *IEEE Trans. Neural Networks and Learning Systems*, vol. 33, no. 5, pp. 1867–1880, May 2022.

[16] Q. Que and M. Belkin, "Back to the future: Radial basis function network revisited," *IEEE Trans. Pattern Analysis and Machine Intelligence*, vol. 42, no. 8, pp. 1856–1867, Aug. 2020.

[17] S. Chen, S. A. Billings, and W. Luo, "Orthogonal least squares methods and their application to non-linear system identification," *Int. J. Control*, vol. 50, no. 5, pp. 1873–1896, 1989.

[18] S. Chen, C. F. N. Cowan, and P. M. Grant, "Orthogonal least squares learning algorithm for radial basis function networks." *IEEE Trans. Neural Networks*, vol. 2, no. 2, pp. 302–309, Mar. 1991.

[19] X. Hong, *et al.*, "Model selection approaches for non-linear system identification: A review," *Int. J. Systems Science*, vol. 39, no. 10, pp. 925–946, Oct. 2008.

[20] S. Chen, X. Hong, and C. J. Harris, "Particle swarm optimization aided orthogonal forward regression for unified data modelling," *IEEE Trans. Evolutionary Computation*, vol. 14, no. 4, pp. 477–499, Aug. 2010.

[21] L. Zhang, K. Li, E. Bai, and G. W. Irwin, "Two-stage orthogonal least squares methods for neural network construction," *IEEE Trans. Neural Networks and Learning Systems*, vol. 26, no. 8, pp. 1608–1621, Sep. 2015.

[22] S. Chen, P. M. Grant, and C. F. N. Cowan, "Orthogonal least squares algorithm for training multi-output radial basis function networks," *IEE Proc. Part F*, vol. 139, no. 6, pp. 378–384, Dec. 1992.

[23] S. Chen, "Multi-output regression using a locally regularised orthogonal least-squares algorithm," *IEE Proc. Vision, Image and Signal Processing*, vol. 149, no. 4, pp. 185–195, Aug. 2002.

[24] S. Chen, X. Hong, and C. .J. Harris "Sparse multioutput radial basis function network construction using combined locally regularised orthogonal least square and D-optimality experimental design," *IEE Proc. Control Theory and Applications*, vol. 150, no. 2, pp. 139–146, Mar. 2003.

[25] S. A. Billings and S. Chen, "The determination of multivariable nonlinear models for dynamic systems," in *Control and Dynamic Systems*, Volume 7 of *Neural Network Systems Techniques and Applications* (ed. C. L. Leondes), San Diego: Academic Press, 1998, pp. 231–278.

[26] D. Du, *et al.*, "A multi-output two-stage locally regularized model construction method using the extreme learning machine," *Neurocomputing*, vol. 128, pp. 104–112, Mar. 2014.

[27] X. Qian, H. Huang, X. Chen, and T. Huang "Generalized hybrid constructive learning algorithm for multioutput RBF networks," *IEEE Trans. Cybernetics*, vol. 47, no. 11, pp. 3634–3648, Nov. 2017.

[28] S. Chen and S. Billings, "Recursive prediction error parameter estimator for non-linear models," *Int. J. Control*, vol. 49, no. 2, pp. 569–594, 1989.

[29] S. Chen, "Nonlinear time series modelling and prediction using Gaussian RBF networks with enhanced clustering and RLS learning," *Electronics Letters*, vol. 31, no. 2, pp. 117–118, Jan. 1995.

[30] N. Liang, G. B. Huang, P. Saratchandran, and N. Sundararajan, "A fast and accurate online sequential learning algorithm for feedforward networks," *IEEE Trans. Neural Networks*, vol. 17, no. 6, pp. 1411–1423, Nov. 2006.

[31] J. Platt, "A resource-allocating network for function interpolation," *Neural Computation*, vol. 3, no. 2, pp. 213–225, Jun. 1991.

[32] G.-B. Huang, P. Saratchandran, and N. Sundararajan, "An efficient sequential learning algorithm for growing and pruning RBF (GAP-RBF) networks," *IEEE Trans. Systems, Man, and Cybernetics, Part B*, vol. 34, no. 6, pp. 2284–2292, Dec. 2004.

[33] H. Chen, Y. Gong, X. Hong, and S. Chen, "A fast adaptive tunable RBF network for nonstationary systems," *IEEE Trans. Cybernetics*, vol. 46, no. 12, pp. 2683–2692, Dec. 2016.

[34] E. S. Chng, S. Chen, and B. Mulgrew, "Gradient radial basis function networks for nonlinear and nonstationary time series prediction," *IEEE Trans. Neural Netw.*, vol. 7, no. 1, pp. 190–194, Jan. 1996.

[35] T. Liu, *et al.*, "Fast adaptive gradient RBF networks for online learning of nonstationary time series," *IEEE Trans. Signal Process.*, vol. 68, pp. 2015–2030, Mar. 2020.

[36] T. Liu, *et al.*, "Fast tunable gradient RBF networks for online modeling of nonlinear and nonstationary dynamic processes," *J. Process Control*, vol. 93, pp. 53–65, Sep. 2020.

[37] G. E. P. Box, G. M. Jenkins, G. C. Reinsel, and G. M. Ljung, *Time Series Analysis: Forecasting and Control* (5th edition). Hoboken, NJ: Wiley, 2015.

[38] D. Lowe, "Adaptive radial basis function nonlinearities, and the problem of generalisation," in *Proc. 1st IEE Int. Conf. Artificial Neural Networks* (London, UK), Oct. 16-18, 1989, pp. 171–175.

[39] L. Wang, Z.-H. You, J.-Q. Li, and Y.-A. Huang, "IMS-CDA: Prediction of CircRNA-disease associations from the integration of multisource similarity information with deep stacked autoencoder model," *IEEE Trans. Cybernetics*, vol. 51, no. 11, pp. 5522–5531, Nov. 2021.

[40] Q. Sun and Z. Ge, "Gated stacked target-related autoencoder: A novel deep feature extraction and layerwise ensemble method for industrial soft sensor application," *IEEE Trans. Cybernetics*, vol. 52, no. 5, pp. 3457–3468, May 2022.

[41] N. Zheng, "Predicting COVID-19 in China using hybrid AI model," *IEEE Trans. Cybernetics*, vol. 50, no. 7, pp. 2891–2904, Jul. 2020.

[42] J. Chen, *et al.*, "E-LSTM-D: A deep learning framework for dynamic network link prediction," *IEEE Trans. Cybernetics*, vol. 51, no. 6, pp. 3699–3712, Jun. 2021.

[43] S. M. Zandavi, T. H. Rashidi, and F. Vafaee, "Dynamic hybrid model to forecast the spread of COVID-19 using LSTM and behavioral models under Uncertainty," *IEEE Trans. Cybernetics*, vol. 52, no. 11, pp. 11977–11989, Nov. 2022.

[44] D. Kingma and J. Ba, "Adam: A method for stochastic optimization," 2014, *arXiv:1412.6980*.

[45] J. Suykens and J .Vandewalle, "Least squares support vector machine classifiers," *Neural Processing Letters*, vol 9, no. 3, pp. 293–300, Jun. 1999.

[46] X. Lu, L. Ming, T. Hu, and B. Fan, "Collaborative learning-based clustered support vector machine for modeling of nonlinear processes subject to noise," *IEEE Trans. Cybernetics*, vol. 50, no. 12, pp. 5162–5171, Dec. 2020.

[47] Q. Ge, *et al.*, "Industrial power load forecasting method based on reinforcement learning and PSO-LSSVM," *IEEE Trans. Cybernetics*, vol. 52, no. 2, pp. 1112–1124, Feb. 2022.

[48] X. Lu and Y. Bai, "Robust least-squares support vector machine using probabilistic inference," *IEEE Trans. Cybernetics*, vol. 52, no. 6, pp. 4391–4399, Jun. 2022.

[49] M. E. Tipping, "Sparse Bayesian learning and the relevance vector machine," *J. Machine Learning Research*, vol 1, pp. 211–244, Jun. 2001.

[50] S. Chen, S. R. Gunn, and C. J. Harris, "The relevance vector machine technique for channel equalization application," *IEEE Trans. Neural Networks*, vol. 12, no. 6, pp. 1529–1532, Nov. 2001.

[51] L. Chen, L. Wang, J. Zhao, and W. Wang, "Relevance vector machines-based time series prediction for incomplete training dataset: Two comparative approaches," *IEEE Trans. Cybernetics*, vol. 51, no. 8, pp. 4298–4311, Aug. 2021.

[52] X. Wang, *et al.*, "Extended relevance vector machine-based remaining useful life prediction for DC-link capacitor in high-speed train," *IEEE Trans. Cybernetics*, vol. 52, no. 9, pp. 9746–9755, Sep. 2022.

[53] E. Spyromitros-Xioufis, G. Tsoumakas, W. Groves, and I. Vlahavas, "Multi-label classification methods for multi-target regression," *arXiv:1211.6581v4*, 2014.

[54] L. Fortuna, S. Graziani, A. Rizzo, and M.G. Xibilia, *Soft Sensors for Monitoring and Control of Industrial Processes*. Springer-Verlag: London, 2007.

[55] U. Jeppsson, *et al.*, "Towards a benchmark simulation model for plant-wide control strategy performance evaluation of WWTPs," *Water Science & Technology*, vol. 53, no. 1, pp. 287–295, Jan. 2006.

[56] Y. Liu, B. Liu, X. Zhao, and M. Xie, "Development of RVM-based multiple-output soft sensors with serial and parallel stacking strategies," *IEEE Trans. Control Systems Technology*, vol. 27, no. 6, pp. 2727–2734, Nov. 2019.